Magnetic Alloys Design Using Multi-objective Optimization

R. Jha [1]

Email rjha001@fiu.edu

G. S. Dulikravich [1,4,*]

Email dulikrav@fiu.edu

M. J. Colaço [2]

Email colaco@asme.org

M. Fan [3]

Email mfan3@ncsu.edu

J. Schwartz [3]

Email Justin_Schwartz@ncsu.edu

C. Koch [3]

Email carl_koch@ncsu.edu

[1] Department of Mechanical and Materials Engineering, Florida International University, Miami, FL, 33174 USA

[2] Department of Mechanical Engineering, Federal University of Rio de Janeiro, UFRJ/COPPE, Rio de Janeiro, Brazil

[3] Department of Materials Science and Engineering, North Carolina State University, Raleigh, NC, USA

[4] MAIDROC Laboratory, Florida International University, 10555 West Flagler Street, EC 3462, Miami, FL, 33174 USA

Abstract

This work presents a computational design of optimal chemical concentrations of chosen alloying elements in creating new magnetic alloys without rare earth elements that have their multiple desired macroscopic properties extremized. The design process is iterative and uses experimental data and a multi-objective evolutionary optimization algorithm combined with a robust response surface generation algorithm. Chemical concentrations of each of the alloying elements in the initial set of candidate alloys were created using a quasi-random sequence generation algorithm. The candidate alloys were then examined for phase equilibria and associated magnetic properties using a thermodynamic database. The most stable candidate alloys were manufactured and tested for macroscopic properties, which were then fitted with response surfaces. The desired magnetic properties were maximized simultaneously by using a multi-objective optimization algorithm. The best predicted Pareto-optimal alloy compositions were manufactured, synthesized and tested thus increasing a set of experimentally verified alloys. This design process converges in a few cycles resulting with alloy chemistries that produce significantly improved desired macroscopic properties, thus proving efficiency of this combined meta-modelling and experimental/computational alloy design method.

Keywords

Alnico alloys
Response surface methodology
Multi-objective optimization
Pareto-optimal
Hierarchical clustering analysis

1. Introduction

Rare-earth elements (REE) are important for the development of high-intensity magnets. Recently, the rare-earth crisis has posed a challenging task in front of the materials research community. Basically, the task is to look for alternate options of synthesizing these magnets and prepare it for application as soon as possible. To address this, one may think of using computational tools to aid experimentalist in order to accelerate this process, [1]. From application point of view, it is important to address a few specific bulk properties: magnetic remanence (B_r), magnetic coercivity (H_c), magnetic energy density (($BH)_{max}$) and Curie temperature. H_c is the ability of a magnet to withstand strong external magnetic field without demagnetizing, [2]. B_r corresponds to the amount of magnetic flux density left in the magnet without demagnetizing. $(BH)_{max}$ is mathematically the area of the largest rectangle that can be inscribed in the second quadrant of the *B-H* curve as shown in Fig. 1, [3]. A high $(BH)_{max}$ means that one can synthesize smaller magnets while maintaining superior magnetic properties. Curie temperature is the temperature above which ferromagnetic behavior disappears as a result of thermal agitation of atoms. Hence, one has to deal with conflicting objectives in order to address the problem.

Fig. 1

B-H curve shows relation between H_c, B_r and $(BH)_{max}$ [3]

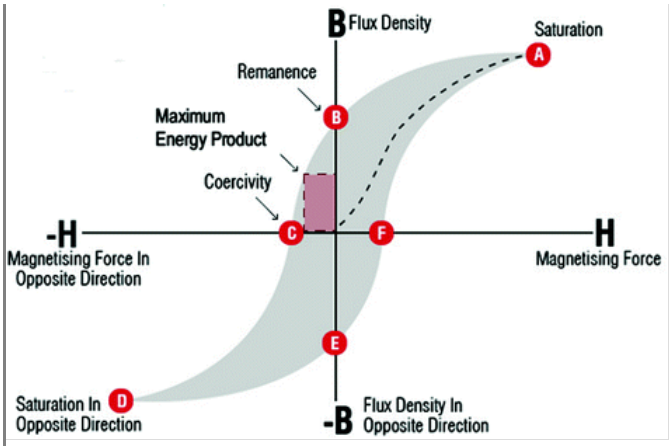

Magnetism is a result of the motion of electrons around the nucleus. The resultant magnetic moment is a result of orbital motion and spin motion. Atoms that have incomplete shells possess permanent magnetic moment. These moments interact with each other and align themselves parallel to each other. At Curie temperature, thermal energy exceeds exchange interaction. Thus, the material loses its magnetic properties and becomes paramagnetic. This phenomenon is observed predominantly in two groups of elements: 3d elements (Cr, Mn, Fe, Co, Ni) and 4f elements (Ce, Nd, Sm, Eu, Gd, Th, Dy, Ho, Er, Tm). 4f elements mentioned here belong to Lanthanides or are also known as rare-earth elements (REE). Ce, Nd, and Sm are light REEs, while Gd and Dy are heavy. Of these, Ce is the most abundant (less critical) while other REEs are critical in terms of supply. REEs have superior magnetic properties due to the presence of 4f electron, [2]. REE based magnets possess very high $(BH)_{max}$, H_c and B_r, [2]. Hence, one can synthesize comparatively smaller magnets without compromising on the magnetic properties. Neodymium based magnets are the strongest available magnets in this family. Samarium–Cobalt based magnets are next to it. Gd and Dy are usually added in varying amounts in order to improve magnetic properties. However, performance of these magnets deteriorates significantly with the rise of temperature. For example, Nd–Fe–B (neodymium–iron–boron) magnets perform the best up to 150 °C [4]. For applications in the range of 150–350 °C, Sm–Co (samarium–cobalt) magnets are usually used. REE-based magnets are susceptible to corrosion and usually need a protective coating in order to prevent corrosion. REE-based magnetic materials are essential in electric cars, in wind turbine electric generators, and any high-efficiency electric devices requiring magnetic fields. Thus, REEs are strategic materials determining which national economies will survive and prosper in the post combustion-engine era. The problem is that deposits of most of the REEs used for synthesizing these magnets are concentrated in a relatively small geographic area. Due to depleting resources and stringent trade rules from the suppliers, it is important to look at other options to synthesize high performance permanent magnets.

Alnico magnets are permanent magnetic alloys predominantly based on the Fe–Co–Ni–Al system without REEs, [2]. Alnico magnets possess very high B_r values that are comparable to REE magnets. Alnico magnets have lower *Hc* values. However, low *Hc* also means that these magnets can be easily magnetized to saturation. A high B_r and low *Hc* value help to cast this material in complex shapes while magnetizing it in the production heat treatment stages. Alnico magnets offer excellent corrosion resistance and high-temperature stability and are the only magnets that can be used up to 800 °C. The excellent high-temperature stability combined with a comparatively higher temperature limits have been successfully exploited by researchers in the past. These properties make it a perfect choice for military and automotive sensor applications. Hence, any improvement in the existing properties of Alnico alloys will help in covering the gap between the Alnico and REE based magnets. This will help in addressing a few important energy conversion applications.

In the present research work, a novel approach is presented for implementation of computational tools (various machine learning algorithms) in design and multi-objective optimization of permanent magnetic Alnico type alloys. The proposed research combines a number of numerical design optimization algorithms with several concepts from artificial intelligence and experimentally evaluated desired properties of an affordable set of candidate alloys. These alloys were further screened by various statistical tools in order to determine various patterns, or any specific trend in the data set. This information will be helpful to the research community in developing a material knowledge base for development of new alloys for targeted properties.

2. Background

At present, researchers around the globe are working on finding alternatives in order to design magnetic alloys that will be able to cover the gap between the properties achieved by Alnico magnets and the rare-earth magnets. An initiative in Europe, Replacement and Original Magnet Engineering Options (ROMEO) program has laid down certain guidelines for researchers that will help to address this topic, [1]. It varies from recycling devices containing rare-earth metals to finding new mines outside China and Russian federation as well as designing magnets without rare-earth additions or with a minimal amount of those rare-earth elements that are less critical in the sense of supply. This will help in addressing a few important energy conversion applications. Sellmyer et al. worked on a few rare-earth free alloys and the properties were found to be in the vicinity of Alnico alloys, [5]. Zhou et al. demonstrated the scope of improvement of magnetic properties of Alnico alloys by theoretical modeling, [6]. However, the difference between the theoretically calculated and the measured properties were quite large for $(BH)_{max}$ and H_c. Hence, random experimentation may be misleading in terms of improvement in alloy properties while being both expensive and time-consuming.

Development of new alloys or even improving the properties of existing alloys is a challenging task mainly due to limited experimental database. Over the years, there has been a growing trend of using machine learning algorithms in materials science, [7–9].

Machine learning algorithms that have been successfully used in materials science domain can be categorized as supervised learning and unsupervised learning algorithms.

- Supervised learning algorithms like neural networks, support vector machines, genetic programming has been successfully used in the past. These algorithms were used to predict processing-structure-property relationship, predict and classify crystal structures, develop model Hamiltonian.

- Unsupervised learning algorithms like principal component analysis (PCA), hierarchical cluster analysis (HCA), *K*-means clustering have been used to address a few important features regarding the dataset. These algorithms can be used to analyze composition spreads, analyze micrographs and noise reduction in the datasets.

A reliable knowledge base for design of new alloys, can be developed by focusing on determining various correlations (composition-property, property-property, composition-composition) from the available databases (simulated and experimental), [10]. This information can be coupled with the theoretical knowledge (atomistic and continuum based theories) to develop the knowledge base. In recent years, integrated computational materials engineering approach along with the materials genome initiative highlights the importance and growing application of computational tools in the development of new alloys, [11]. It aims at reducing a new alloy development cycle from currently 10 years to two years or even less. Various data-driven techniques combined with evolutionary approaches have been successfully implemented in alloy design and also in improving thermodynamic databases such as ThermoCalc for alloy development, [7, 8, 12–16]. Data mining approaches such as PCA and partial least square (PLS) regression have been successfully used in designing new alloys, [17], as well as determining properties of element Lutetium, [18]. These applications demonstrate the efficacy of application of computational tools for materials design. This acted as motivation for us in proceeding forward to design our own approach for design and optimization of magnetic alloys.

In this work, we will be using a number of machine learning algorithms. We will be using the response surface methodology approach to develop meta-models that will link the bulk properties to the chemical composition. Multi-objective optimization of targeted properties will be done in order to predict the next set of alloys, basically by using various algorithms based on evolutionary approaches. Data analysis will be performed to discover various patterns within the dataset by using various statistical tools.

2.1. Alnico Magnets

Alnico magnets were discovered in 1931 by Mishima in Japan [2, 3]. These magnets were based on the Fe–Co–Ni–Al system. Magnetic properties in these magnets were attributed to the presence of a two-phase system of body centered cubic (BCC), α_1 and α_2. In later years, it was observed that separation of α_1 and α_2 is due to a metallurgical phenomenon popularly known as “Spinodal” decomposition. α_1 is Fe–Co rich ferromagnetic phase, while α_2 is Ni–Al rich phase. These phases are stable up to 850 °C (Curie temperature is about 860 °C). Above 850 °C, the face centered cubic (FCC) phase begins to appear. FCC phase is quite detrimental for magnetic properties. In the past, an FCC γ phase was observed in a few compositions [3]. In later years, various attempts were made to stabilize the magnetic α_1 and α_2 phases, while at the same time eliminate or reduce the amount of FCC γ phase. These attempts include modification of heat treatment protocol and addition of other alloying elements to enhance various magnetic properties of these materials. Due to the discovery of powerful REE-based magnets, there has been limited research on Alnico magnets after 1980. The recent rise in prices of rare earth elements led to the search magnets that are free of REEs and has motivated researchers to work on improving magnetic properties of Alnico magnets. Due to their proven high-temperature stability and related properties, Alnico magnets are a popular choice for research.

Currently, Alnico alloys contain 8+ elements. Calphad approach can successfully handle ternary or at most quaternary systems [19]. This makes this work even more complicated. In our work, we used 8 alloying elements on the basis of available literature and mutual discussion. These elements include iron (Fe), cobalt (Co), nickel (Ni), aluminum (Al), titanium (Ti), hafnium (Hf), copper (Cu) and niobium (Nb). Variable bounds of these elements have been tabulated in Table 1. It is important to know the role of these alloying elements initially for the manufacture of alloys for targeted properties. Later, this information can be utilized to select a meta-model for a certain property. This is done with a purpose to develop a knowledge base for discovery of new materials while improving properties of existing materials. $(BH)_{max}$ is mathematically the area of the largest rectangle that can be inscribed in the second quadrant of the *B*-*H* curve as shown in Fig. 1. Coercivity and remanence are conflicting that is one has to sacrifice on one of these properties to improve the other property. Therefore, in order to increase $(BH)_{max}$, one needs to optimize H_c and B_r. Hence, multi-objective optimization will prove to be an asset to address this problem.

Table 1

Concentration bounds AlNiCo type alloys

	Variable bounds (wt%)		
Alloying elements	1–85	86–143	144–180
Cobalt (Co)	24–40	24–38	22.8–39.9
Nickel (Ni)	13–15	13–15	12.35–15.75
Aluminum (Al)	7–9	7–12	6.65–12.6
Titanium (Ti)	0.1–8	4–11	3.8–11.55
Hafnium (Hf)	0.1–8	0.1–3	0.095–3.15
Copper (Cu)	0–6	0–3	0–4.5
Niobium (Nb)	0–2	0–1	0–1.5
Iron (Fe)	Balance to 100		

Role of various alloying elements and their effects on H_c and B_r have been addressed by Dilon [3] and are summarized here.

1. Cobalt is a γ stabilizer. Hence, a solutionization anneal is needed to homogenize it to a single phase. It increases H_c and Curie temperature.
2. Nickel is also a γ stabilizer. Hence, a higher solutionization anneal temperature is needed to homogenize the gamma phase. It increases H_c (less than

cobalt) but, at the expense of B_r.

3. Aluminum is an α stabilizer. Hence, it will help in reducing the solutionization temperature. It affects H_c positively.

4. Copper is an α stabilizer. It increases H_c and B_r. In Alnico 8 and 9 alloys, Cu precipitates out of the α_2 phases into particles and increases the magnetic separation between α_1 and α_2 phases. It results in an increase in H_c. In Alnico 5–7 alloys, Cu remains in α_2. It leads to an increase in H_c while a decrease in Curie temperature.

5. Titanium is also an α stabilizer. It is one of the most reactive elements. It reacts with impurities such as S and N and precipitates out thus purifying the magnet. It also eliminates carbon which is a strong γ stabilizer and needs to be eliminated at any cost. Titanium helps in grain refining and inhibits columnar grain growth. Due to columnar grain growth, majority of grains are aligned perpendicular to the chill plate. Large shape anisotropy can be achieved if spinodal decomposition occurs in this direction. Titanium increases H_c while it decreases B_r.

6. Niobium is also an α stabilizer. It helps in neutralizing the effects of carbon. Like titanium, Nb inhibits columnar grain growth. Nb increases H_c, while it decreases B_r. However, the decrease in B_r due to Nb is less than that observed due to Ti.

7. Hafnium is used for enhancing high-temperature properties. Hf usually precipitates at the grain boundary and helps in improving creep properties. Recent studies related to Co–Hf magnets motivated us to use Hf in this work, [20].

3. Current Research

In this work, we used a set of computational tools to develop a novel approach for design and optimization of high-temperature, high-intensity magnetic alloys, [15]. The steps involved in the proposed approach can be listed as follows.

1. Initial dataset: From the open literature and our expertise, we defined the concentration bounds of 8 alloying elements that we used to create alloy. Within these bounds, we used a well-known quasi-random sequence generator [25], to generate chemical concentrations for each of the initial 80 candidate alloys (see Tables 1 and 2). The initial set of alloys was screened on the basis of limited knowledge of phase equilibrium and magnetic property from a commercial thermodynamic database, Factsage [21].

Table 2

Cycle and alloy number

Cycle number	Alloys designed	Best alloy (number)
1	1–80	30
2	81–85	84
3	86–90	86
4	91–110	95
5	111–120	117
6	120–138	124
7	139–143	139
8	144–150	150
9	151–160	157
10	161–165	162
11	166–173	169
12	174–180	180

2. Manufacture and testing: The alloys were manufactured and tested for various properties of interest as shown in Table 3 . This work was performed at North Carolina State University.

Table 3

Quantities to be simultaneously extremized using multi-objective optimization

	Properties	Units	Objective
1	Magnetic energy density ($(BH)_{max}$)	Kg m^{-1} s^{-2}	Maximize
2	Magnetic coercivity (H_c)	Oersted	Maximize
3	Magnetic remanence (B_r)	Tesla	Maximize

	Properties	Units	Objective
4	Saturation magnetization (M_s)	Emu/g	Maximize
5	Remanence magnetization (M_r)	Emu/g	Maximize
6	$((BH)_{max})$/mass	$m^{-1}\ s^{-2}$	Maximize
7	Magnetic permeability (μ)	Kg m $A^{-2}\ s^{-2}$	Maximize
8	Cost of raw material (*cost*)	USD/Kg	Minimize
9	Intrinsic coercive field (*jHc*)	A m^{-1}	Maximize
10	Density(ρ)	Kg m^{-3}	Minimize

3. Response surface generation: From the available data, response surfaces were developed for the measured and calculated properties listed in Table 3. We used a commercial optimization package, modeFRONTIER for this purpose [22]. The response surfaces were developed using the following algorithms: Radial basis functions (RBF), Kriging, Anisotropic Kriging and Evolutionary Design. Each response surface was tested using various accuracy measures and the most accurate one was chosen for further study.

4. Multi-objective optimization: The most accurate response surfaces were used to extremize the various properties as per the objectives specified in Table 3. Several optimization runs were performed to get a diverse pool of results. The optimization algorithms used in modeFRONTIER were: Non-dominated Sorting Genetic Algorithm II (NSGA2), Multi-Objective Particle Swarm Optimization (MOPSO), Multi-Objective Simulated Annealing (MOSA) and FAST optimizer (FAST uses response surface models (meta-models) to speed up the optimization process using various algorithms like NSGA2, MOPSO, MOSA), [22]. Besides modeFRONTIER optimization software, we also used IOSO optimization software [7], an in-house hybrid response surface generation algorithm [23, 24] and a surrogate model selection algorithm [24]. Predictions from the optimization packages were merged and a set of Pareto-optimized alloy concentrations were selected for manufacture and testing.

5. The computational-experimental work was performed in cycles to check upon improvements over the previous cycles. Steps 2–2 were repeated until the improvements of multiple macroscopic properties of such magnetic alloys become negligible in consecutive cycles.

6. Sensitivity analysis: Various statistical tools were used to determine composition-property relations. This was done in order to find the most and the least influential alloying element so as to make way for possible single affordable rare-earth element addition.

7. Hierarchical cluster analysis (HCA) was used to determine pattern in the dataset as a whole and in the clusters as well. This can be used to screen alloys before manufacture.

This work is aimed at developing a knowledge base that will motivate experimentalists to make modifications in standard manufacture protocols for improvements. This will also help the research community in designing new alloys for targeted properties. In data-driven material science, one needs to focus upon a few key factors that will help in developing knowledge base for designing new materials, [10]:

1. Data: Our database is a combination of experimentally verified data predicted by a well-known random number generator and data from Pareto-optimized predictions as discussed above.

2. Correlations: Dataset was examined by a set of statistical tools and various linear and non-linear correlation, hierarchical clustering analysis, and principal component analysis tool to discover various trends in the dataset.

3. Theory: This information can be coupled with theoretical knowledge to motivate the experimentalists to move forward with the manufacture of new alloys.

4. Results

At present, we have worked through 12 cycles of design and optimization followed by experimental validation. Table 2 lists the alloys manufactured in each of the cycles and the best alloy in each cycle ranked on the basis of $(BH)_{max}$ values. Work done in all the cycles are described as follows:

1. Cycle 1 (Alloys 1–80): As discussed in Sect. 3, initial chemical compositions were predicted randomly by Sobol's algorithm [25]. A set of 80 such candidate compositions was manufactured and macroscopic properties of each of these alloys measured.

2. Cycle 2 (Alloys 81–85): Using experimentally measured properties of these 80 initial alloys, response surfaces were created and multi-objective optimization was performed resulting in 5 new Pareto-optimized chemical compositions. These 5 predicted compositions were manufactured and their macroscopic properties measured. It was observed that one of the predicted alloys (alloy 84) outperformed the initial set of alloys and the other Pareto-optimized alloys. This demonstrates the efficacy of the current approach in using computational tools in materials design. The bounds on chemical concentrations of alloying elements were modified (Table 1) to accelerate the design.

3. Cycle 3 (Alloys 86–90): Using experimentally measured properties of the 80 + 5 alloys, response surfaces were created and multi-objective optimization was performed resulting in 5 new Pareto-optimized chemical compositions. These 5 predicted chemical compositions were manufactured and their macroscopic properties measured. In this cycle, alloy 86 was the best candidate. It was observed that the measured properties of the new set (alloys 86–90) were in the vicinity of the previous set of alloys. This can be attributed to non-uniform distribution of some of alloying

elements in the initial set of 80 candidate compositions which was due to an oversight on the part of users of the random sequence generator. This negatively affected the accuracy of the response surfaces resulting in no significant improvement over the previous cycle.

4. Cycle 4 (Alloys 91–110): Therefore, next set of 20 alloys were randomly predicted by Sobol's algorithm [25] specifically to improve the uniformity of distribution of concentrations of the 8 alloying elements. This provided response surfaces with more uniform support in the eight-dimensional variable space. These 20 random alloys were manufactured and their macroscopic properties measured. In this cycle, alloy 95 was the best performer. Alloy 95 had an H_c of 980 Oe (as compared to 750 Oe for the previous best alloy 84).

5. Cycle 5 (Alloys 111–120): Using measured values of the macroscopic properties of the 110 alloys, response surfaces were created and multi-objective optimization was performed resulting in 10 new Pareto-optimized alloys. These 10 chemical compositions were then manufactured and their properties measured. We observed significant improvements in the properties of the new alloys. Alloy 111 and 114 had H_c of 1050 Oe and alloy 117 reported 1000 Oe (as compared to 980 Oe for the previous best alloy 95). In this cycle, alloy 117 was the best alloy in terms of $(BH)_{max}$.

6. Cycle 6 (Alloys 121–138): Using measured values of the macroscopic properties of the 120 alloys, response surfaces were created and multi-objective optimization was performed resulting in 18 new Pareto-optimized alloys. These 18 alloys were then manufactured and their properties measured. In this cycle, alloy 124 was the best performer. We observed significant improvement in both $(BH)_{max}$ and H_c.

7. Cycle 7 (Alloys 139–143): Using measured values of the macroscopic properties of the 138 alloys, response surfaces were created and multi-objective optimization was performed resulting in 5 new Pareto-optimized alloys. These 5 alloys were then manufactured and their properties measured. In this cycle, alloy 139 was the best performer, although its properties were in the vicinity of alloy 124. Since there was no significant improvement in the desired properties, design and optimization task was halted at this point to minimize waste of resources and funding. There was a clear need to perform a sensitivity analysis of the variables and associated properties as well as to test a hybrid response surface [24]. Consequently, in cycles 8–11 (Alloys 144–180) bounds on concentrations of each of the alloying elements were relaxed by 5 %, while the overall methodology remained the same (as mentioned in Sect. 3).

8. Cycle 8 (Alloys 144–150): Using modeFRONTIER software there was a marginal improvement in H_c, with no improvement in other properties of new alloys.

9. Cycle 9 (Alloys 151–160): using surrogate model selection algorithm (SM), no significant improvement was observed in this cycle for any of the properties discussed in Table 3.

10. Cycle 10 (Alloys 161–165): Using modeFRONTIER software there was a marginal improvement in H_c.

11. Cycle 11 (Alloys 166–173): Using a hybrid response surface and modeFRONTIER software there was a marginal improvement in H_c, with no improvement in other properties.

12. Cycle 12 (Alloys 173–180): Using a hybrid response surface and modeFRONTIER software, there was a marginal improvement in H_c, with no improvement in other properties.

Figures 2, 3 and 4 show the comparison between various approaches for several macroscopic properties of alloys created in this work. These figures demonstrate that the alloys predicted by meta-modeling and multi-objective optimization dominate the ones predicted by random design approach either by Sobol's algorithm or a human brain. The achieved properties improved in consecutive cycles: H_c values are at par with commercial alloys [6], while further improvements in $(BH)_{max}$ and B_r values are expected in the next few cycles. Hence, sensitivity analysis of the response surfaces and pattern recognition in the dataset need to be performed at this point.

Fig. 2

Magnetic energy density versus magnetic coercivity

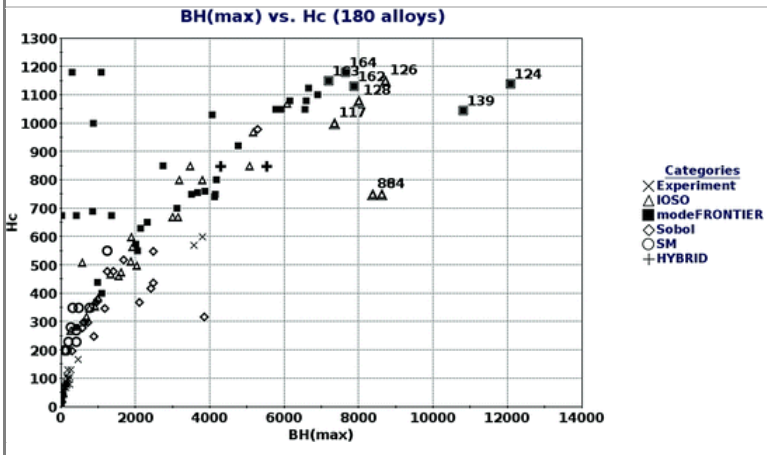

Fig. 3

Magnetic energy density versus magnetic remanence, comparison of solutions by various approaches

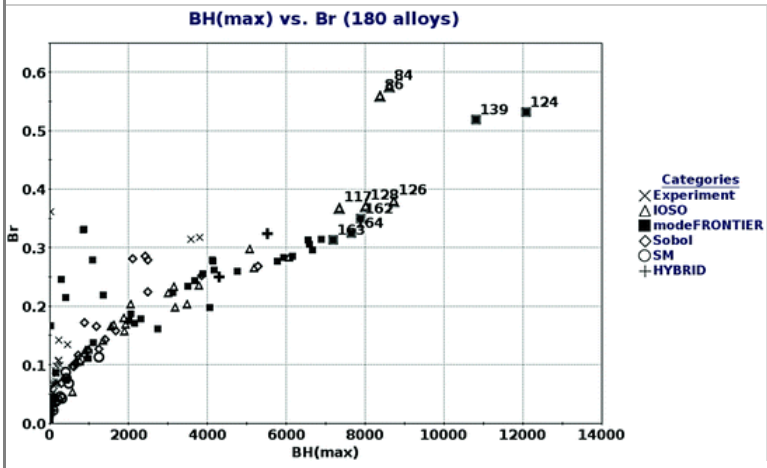

Fig. 4

Magnetic coercivity versus magnetic remanence, comparison of solutions by various approaches

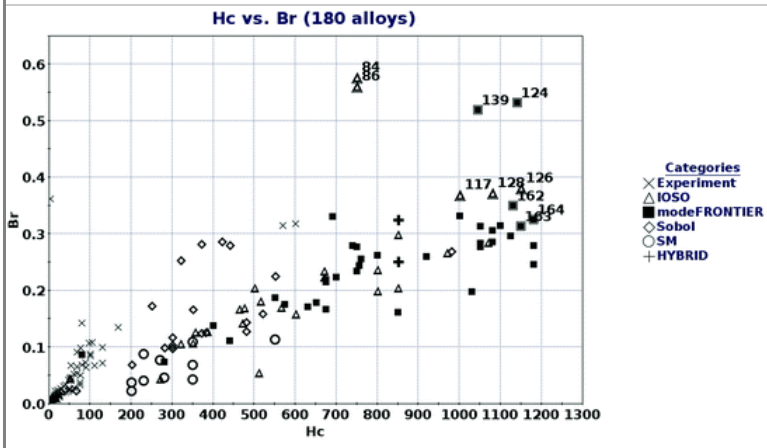

5. Sensitivity Analysis

This was done in order to establish/determine the composition-property relationship, find various trends and patterns within the dataset. Initially, Pearson's linear correlation method was used (not reported here), [15]. Coefficients were too low. This was expected as the dataset is quite noisy. A few other statistical measures used to address this issue are discussed below.

5.1. Single Variable Response (SVR)

SVR has been used in the past for qualitative analysis of the training results obtained from evolutionary neural network [26] and bi-objective genetic programming, [16, 27]. Here, a trend of variation is created by generating values between 0 and 1 on a time scale. The trend line is intentionally made irregular so that there are regions of constant values, sharp increases, and sharp decreases in the line. This is done to emulate non-linear behavior of the dataset. It has been referred to as an input signal in the following text. This input signal (a trend of variation) was used for one of the variables (concentration of one of the alloying chemical elements), while the other variables were kept constant at an average value. The various responses were tabulated in Table 4 for each of the models. Following terminologies were used for the responses:

Table 4

Single variable response for various properties

Sl. no.	Single variable response (SVR)								
	Properties	Fe	Co	Ni	Al	Ti	Hf	Cu	Nb
1	$(BH)_{max}$	Nil	Nil	Mixed	Nil	Nil	Nil	Nil	Nil
2	H_c	Mixed	Mixed	Mixed	Inverse	Mixed	Direct	Direct	Mixed
3	B_r	Mixed	Mixed	Mixed	Inverse	Mixed	Direct	Direct	Inverse

Sl. no.	Single variable response (SVR)								
	Properties	**Fe**	**Co**	**Ni**	**Al**	**Ti**	**Hf**	**Cu**	**Nb**
4	M_s	Direct	Inverse	Direct	Mixed	Inverse	Direct	Mixed	Mixed
5	M_r	Nil	Nil	Nil	Nil	Nil	Nil	Nil	Nil
6	$(BH)_{max}$/mass	Nil	Nil	Nil	Nil	Nil	Nil	Nil	Nil
7	m	Mixed	Mixed	Mixed	Mixed	Inverse	Mixed	Mixed	Mixed
8	*cost*	Inverse	Inverse	Inverse	Direct	Direct	Direct	Inverse	Direct
9	jH_c	Mixed	Mixed	Mixed	Inverse	Inverse	Mixed	Direct	Mixed
10	ρ	Mixed	Direct	Mixed	Inverse	Inverse	Mixed	Mixed	Direct

- Direct: In this case, the model output increases by increasing the value of an input signal and decreases on decreasing the value.
- Inverse: In this case, a particular variable will affect the model output in an opposite manner.
- Nil: This means that the model was unable to find any correlation between that particular variable and the model output.
- Mixed: In this case, the model has a different response for a different set of data of any particular variable.

Since current experimental dataset is quite noisy, the SVR analysis resulted in many mixed responses. However, a few important findings can be listed as follows.

1. Copper shows a direct response for H_c and B_r, thus response surface predictions are at par with available literature, [3]. This has been discussed earlier in Sect. 2.1.
2. Hafnium shows a direct response for H_c and B_r. Hf has not been previously used in Alnico alloys. Hence, further data analysis is required before reaching a final conclusion.
3. Nickel shows mixed response with $(BH)_{max}$.

Thus, meta-modeling can prove to be an asset for developing alloys in future as well as in predicting the properties of alloys with a new composition. We moved forward to analyze the dataset by few other machine learning tools in order to cross check our findings.

5.2. Hierarchical Cluster Analysis (HCA)

Clustering analysis is usually performed to find a pattern in a dataset. A cluster consists of data points which are similar to the other data points within the same cluster, while dissimilar to data points in the other clusters. In most cases, the similarity criterion is the Euclidian distance between the data points.

In HCA, clustering begins with each data point within a cluster [9, 22]. These clusters are iteratively merged to form larger ones and finally merged into one large cluster. In this work, clustering was done by Ward's approach while there are several other alternatives for the same [22, 28]. The final result is a tree like structure referred to as "dendrogram", which shows the way the clusters are related. The user can specify a distance or number of clusters to view the dataset in disjoint groups. In this way, the user can eliminate a cluster that does not serve any purpose as per his expertise.

In this case, we used multivariate data analysis (MVA) node in optimization package: modeFRONTIER [22] and another statistical software known as IBM SPSS [28] for HCA analysis. The alloys were clustered on the basis of targeted properties. Dendrogram was cut in a manner so that it results in a total of 9 clusters (Cluster 0 to Cluster 8) as denoted by the numbers in the dendrogram plot. Figure 5 shows the dendrogram plot obtained from HCA analysis. Cluster 8 and cluster 7 were merged as one when analyzed by Ward's approach. Clustering parameters and the number of alloys included in each cluster have been tabulated in Table 5.

Fig. 5

Dendrogram plot from HCA analysis

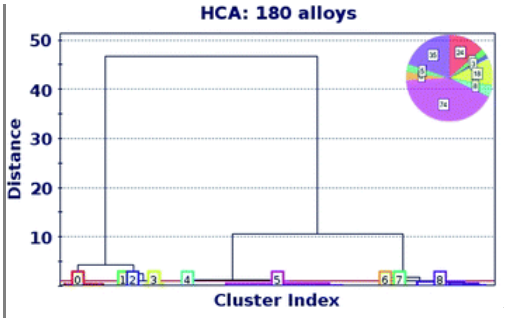

Table 5

Clustering parameters in HCA analysis

Cluster number	Cluster size	ISim	ESim	Best alloy
0	24	2.5	1.1	175,115
1	4	1.5	0.6	84, 86, 124, 139
2	3	1.5	0.7	145, 146, 147
3	18	3.2	0.8	117, 126, 128
4	8	4.5	1.3	
5	74	4.6	1.0	
6	6	1.7	1.0	
7	40	2.1	1.3	

Clusters are classified by the following measures [22].

1. Internal similarity (ISim): It reflects the compactness of the *k*th cluster. It must be higher.
2. External similarity (ESim): It reflects the uniqueness of *k*th cluster. It must be lower.
3. Descriptive variables: These are the most significant variables that help in identifying cluster elements that are similar to one another.
4. Discriminating variables: These are the most significant variables that help in identifying cluster elements that are dissimilar to other clusters.

From Table 5, we can see that cluster 1, cluster 2 and cluster 3 have higher Isim, while a lower Esim when compared to other clusters. Cluster 1 and cluster 3 contain top 10 alloys based on $(BH)_{max}$ value, while alloys in cluster 2 possess high H_c.

HCA analysis can be used to cross-check the findings of SVR analysis mentioned above in the text. The following text includes cluster scatter plots for various elements versus $(BH)_{max}$, H_c and B_r followed by relevant information extracted from them. In the following figures, confidence level for both the confidence interval and confidence ellipse is 0.9. These figures can be helpful in determining the variable bounds for targeted properties.

In Fig. 6, for cluster 1, $(BH)_{max}$ increases with decrease in aluminum content in the range 6–10 wt%. Other clusters have mixed response for variation of aluminum.

Fig. 6

Clusters scatter: $(BH)_{max}$ versus aluminum concentration

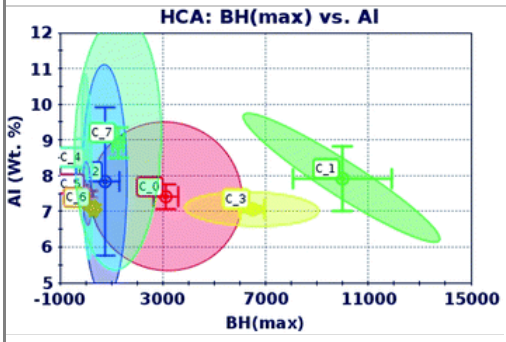

It can be seen from Fig. 7 that H_c increases with an increase in Cu content in cluster 1 and cluster 3, while H_c, decreases with increasing Cu content in cluster 2 in a narrow composition range. Overall, copper affects H_c positively, and this is know from the literature (Sect. 2.1) as well as SVR analysis (Sect. 5.1).

Fig. 7

Cluster scatter: H_c versus copper concentration

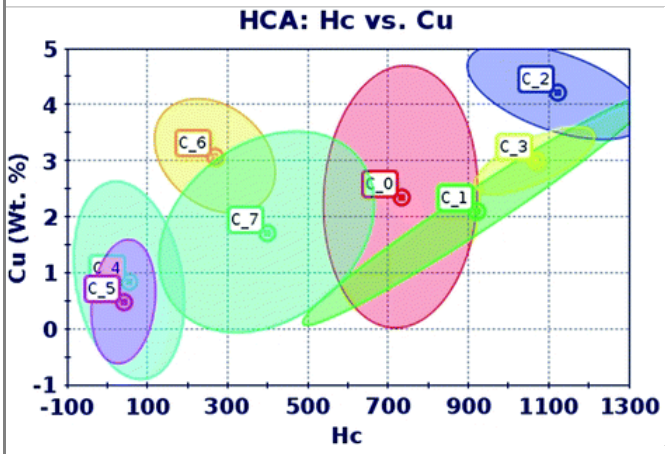

From Fig. 8, it is difficult to determine the role of Cu addition on B_r. From literature (Sect. 2.1) as well as SVR analysis (Sect. 5.1, Cu tends to affect B_r positively. Hence, this needs further investigation.

Fig. 8

Cluster scatter: B_r versus copper concentration

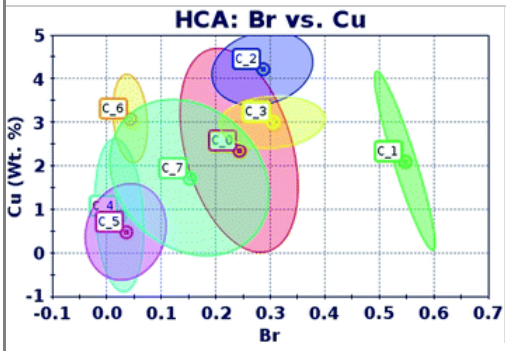

Figure 9 shows scatter plot for $(BH)_{max}$ versus copper for various clusters. This behavior was expected as B_r and H_c are conflicting (see Figs. 1, 7 and 8). It is difficult to determine the role of Cu addition from $(BH)_{max}$ versus Cu plot.

Fig. 9

Clusters scatter: $(BH)_{max}$ versus copper concentration

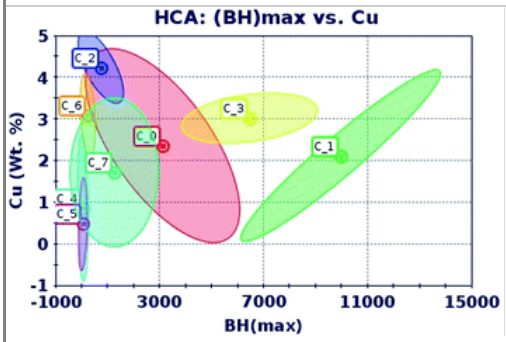

From Fig. 10, one can observe that in cluster 2 and cluster 7, H_c tends to increase with an increase in Ti content.

Fig. 10

Clusters scatter: H_c versus titanium concentration

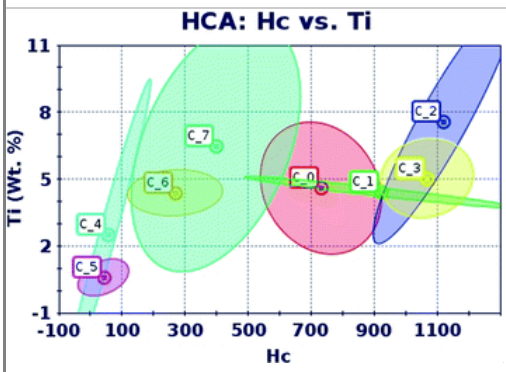

From Fig. 11, it can be seen that in order to increase $(BH)_{max}$, one needs to stay in a narrow concentration range for Fe.

Fig. 11

Clusters scatter: $(BH)_{max}$ versus iron concentration

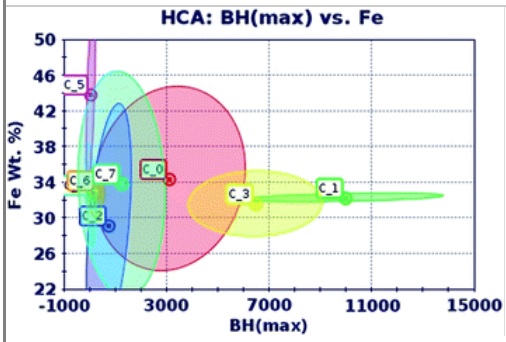

Nickel showed a weak response for $(BH)_{max}$ in SVR analysis (Sect. 5.1). Hence, we plotted scatter plots for Ni versus $(BH)_{max}$. From Fig. 12, it can be observed that in cluster 1, $(BH)_{max}$ increases with decrease in Ni content. This can also be observed in cluster 2.

Fig. 12

Clusters scatter: $(BH)_{max}$ versus nickel concentration

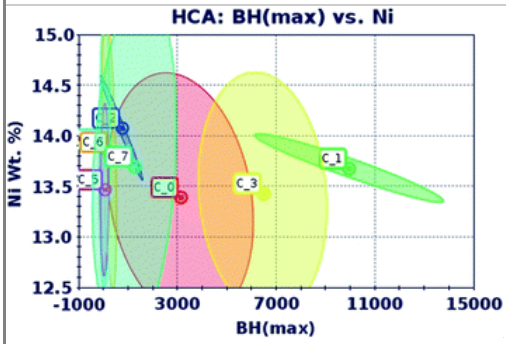

One can also use these plots for discarding a few alloying elements in order to make way for REE addition. We plotted scatter plots for niobium versus $(BH)_{max}$, H_c and B_r with this objective in mind. From Figs. 13, 14 and 15, one can see that Nb is almost neutral to H_c and B_r. This was also observed in SVR analysis (Sect. 5.1). Additionally, Nb has the same effect as Ti (Sect. 2.1). Hence, one can think of manufacturing a few samples without Nb. Or, replacing Nb and with a REE.

Fig. 13

Clusters scatter: H_c versus niobium concentration

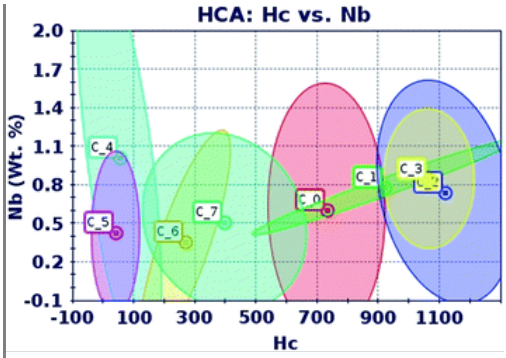

Fig. 14

Clusters scatter: B_r versus niobium concentration

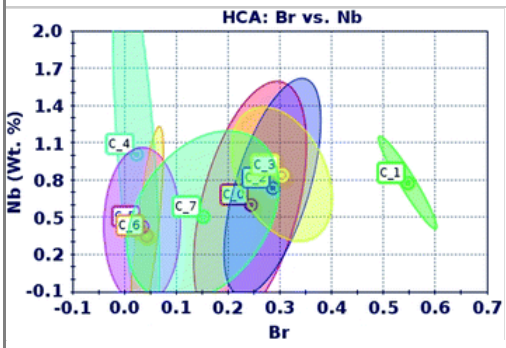

Fig. 15

Clusters scatter: $(BH)_{max}$ versus niobium concentration

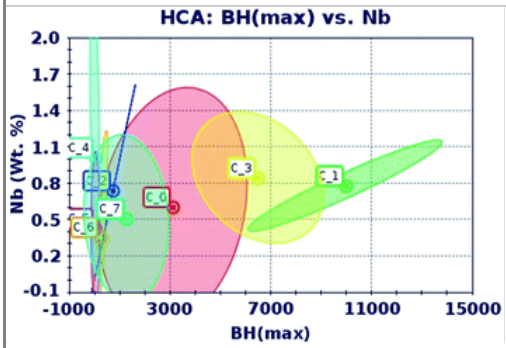

5.3. Thermodynamic Analysis

In this research, we have been using 8 alloying elements. Hence, it will be helpful for the experimentalists to have some information regarding the stability of critical phases during manufacture and designing heat treatment protocols. In this work, we studied phase stability of a few Alnico type alloys from 0 to 1200 °C using Factsage software [21]. The resulting diagrams are based on equilibrium calculation, hence the final experimental results may be different. However, these diagrams can be used as a guideline for the experimentalists when selecting alloys prior to manufacture [16, 29].

From Fig. 16, it can be observed that alloy 124 is thermodynamically stable up to 800 °C, while in alloys 84, 86 and 126 transformation (BCC-FCC) starts at a lower temperature. Hence, the experimentalists can design a heat treatment protocol so they can avoid transformations that will have a detrimental effect on the magnetic properties. We extended this analysis by modifying the composition of alloy 124. We added Mn in various amounts and plotted the critical phases.

Fig. 16

Phase distribution diagrams for alloy **a** 84, **b** 86, **c** 124 and **d** 126

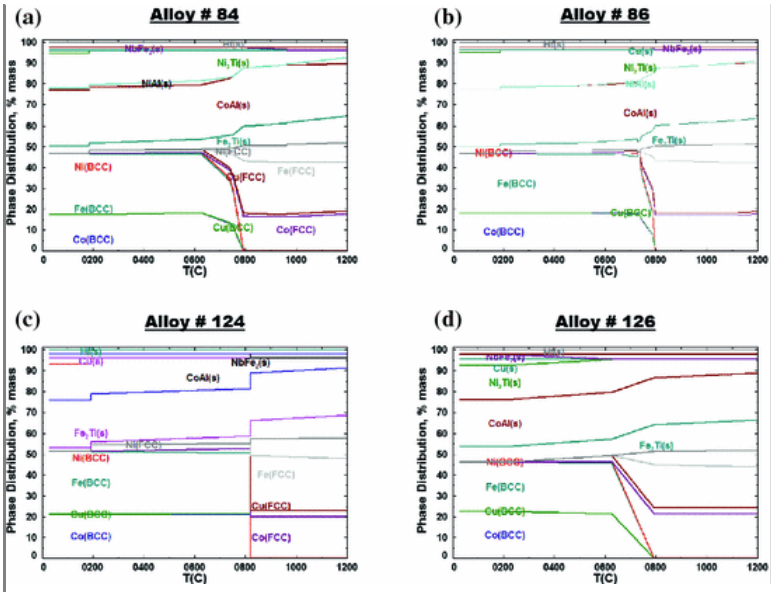

From Fig. 17, it can be seen that these additions had detrimental effect and BCC-FCC transformation starting well below 800 °C. Consequently, at this point we can say that Alnico type alloys should not have any Mn and B addition.

Fig. 17

Phase distribution diagram obtained after modifying composition of alloy 124 **a** 0.5 g Mn added to alloy 124, **b** 1.0 g Mn added to alloy 124, **c** 0.5 g Mn added to alloy 124 and Nb removed, and **d** 1.0 g Mn and 0.5 g of B added to alloy 124

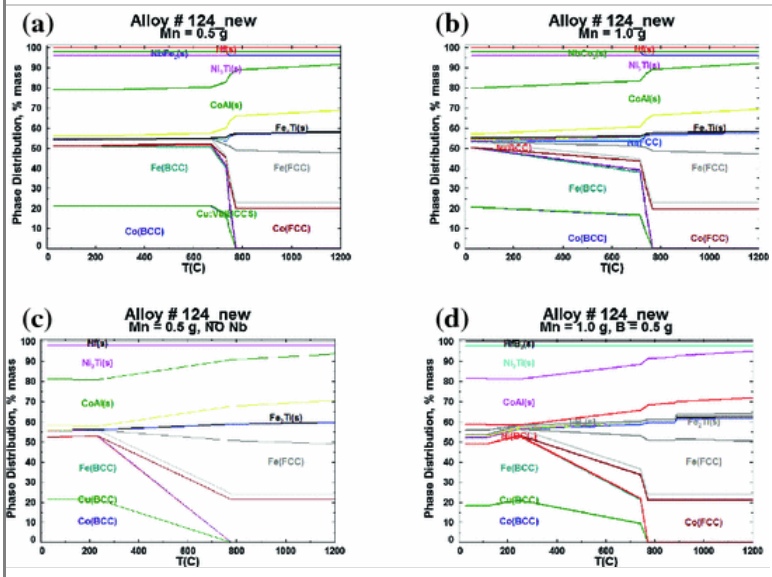

6. Discussions

Figures 2, 3 and 4 show the scatter plots of magnetic energy density versus magnetic coercivity and magnetic remanence. Top 10 alloys are marked on the figure. Alloys were ranked on the basis of $(BH)_{max}$ values in Figs. 2, 3 and 4 and Table 2. So far, the best alloy is alloy 124 and its composition was predicted computationally in MAIDROC laboratory at Florida International University. Figures 2, 3 and 4 demonstrate the efficacy of the present approach. Pareto-optimized predictions (using modeFRONTIER, IOSO and HYBRID approach) dominate the initial 80 candidate alloys as well as most of those predicted by the random number generator Sobol's algorithm in later stages. The present alloy development time was approximately one year which is significantly less than the time needed to design new alloys using standard procedures. In order to improve from the initial set of 80 alloys to the current best, the time frame was only 5 months. Moreover, our computational design approach was able to successfully recover from the initial flaws. This would have been impossible by random experimentation. One peculiar finding in this work is that we were able to achieve an increase in H_c without compromising on B_r.

Cu shows a direct correlation with H_c and B_r which can be confirmed from the literature (Sect. 2.1). Hf seems to affect H_c and B_r positively. H_c increases with an increase in Cu content. This was observed in SVR analysis (Sect. 5.1), as well as from the literature (Sect. 2.1). Nickel shows mixed response for $(BH)_{max}$ as observed in SVR analysis (Sect. 5.1). Titanium showed mixed response for H_c in SVR analysis. In HCA analysis, we observed an increase in H_c values with an increase in Ti content. From the above analysis, we can conclude that we can remove niobium in order to make way for the rare-earth addition.

Thermodynamic analysis can prove to be helpful in designing heat treatment protocols. Hence, an initial study shows promising results. There is scope for improvement in the accuracy of response surface predictions, equilibrium calculations and HCA which can be used to screen a few alloys prior to manufacture.

7. Conclusions

One of the main purposes of computational materials science is to motivate experimentalists to incorporate a few modifications in the standard alloy development protocols for improved results. In this work, we demonstrated that it is possible to start the alloy design optimization process without any expertise in the design of alloys and to rapidly develop/improve alloys during several design cycles requiring an affordable number of alloys to be manufactured and tested. Even though our first set of results were not per our expectations due to a human error in the design process, the interactive computational/experimental design procedure was able to rapidly recover from it. We were able to improve these properties by an order of magnitude by meta-modeling and multi-objective optimization. Obtained results were screened by using standard statistical tools and the entire design procedure utilized multiple concepts of machine learning to come at a meaningful conclusion. The experimental dataset was quite noisy at the same time we were dealing with a multi-component system. Hence, non-linear composition-property relation was expected. Several such correlations known from the open literature were also proven in this work. For other correlations, we need to do further experiments. Screening of alloys on the basis of thermodynamic analysis from a limited database is another positive outcome of this work. Other query from the experimentalists can be addressed by modifying our algorithms.

8. Future Work

Based on the experience learned while developing this computational/experimental alloy design optimization methodology, it can be recommended that future work include the following items.

1. Improve response surface accuracy.
2. Introduce uncertainty in response surface predictions.
3. Microstructure and texture study.
4. Design an optimal temperature versus time heat treatment protocol for simultaneously with the design of the optimal chemical composition of the alloy.

Acknowledgements

Authors would like to express their gratitude to Prof. Carlo Poloni, founder and president of ESTECO, for providing modeFRONTIER software free of charge for this project. They would also like to express their gratitude to Prof. Igor N. Egorov, founder and president of IOSO Technologies, for providing IOSO software free of charge and for performing some of the preliminary calculations. This work was funded by the US Air Force Office of Scientific Research under grant FA9550-12-1-0440 monitored by Dr. Ali Sayir. The views and conclusions contained herein are those of the authors and should not be interpreted as necessarily representing the official policies or endorsements, either expressed or implied, of the US Air Force Office of Scientific Research or the U.S. Government. The U.S. Government is authorized to reproduce and distribute reprints for government purposes notwithstanding any copyright notation thereon.

References

1. Mcguiness P, Akdogan O, Asali A, Bance S, Bittner F, Coey JMD, Dempsey NM, Fidler J, Givord D, Gutfleisch O, Katter M, Le Roy D, Sanvito S, Schrefl T, Schultz L, Schwöbl C, Soderžnik M, Šturm S, Tozman P, Űstűner K, Venkatesan M, Woodcock TG, Žagar K, Kobe S (2015) JOM 67:1306 **AQ1**
2. Cullity B, Graham C (2009) Introduction to magnetic materials. Wiley-IEEE Press, New York
3. Dilon H (2014) Master thesis, Iowa State University, USA
4. Kramer MJ, McCallum RW, Anderson IA, Constantinides S (2012) JOM 64:752
5. Sellmyer DJ, Balamurugan B, Zhang WY, Das B, Skomski R, Kharel P, Liu Y (2013) In: The 8th Pacific rim international congress on advanced materials and processing. Wiley, Hoboken
6. Zhou L, Miller M, Lu P, Ke L, Skomski R, Dillon H, Xing Q, Palasyuk A, McCartney M, Smith D, Constantinides S, McCallum R, Anderson I (2014) Acta Mater 74:224
7. Egorov-Yegorov IN, Dulikravich GS (2005) Mater Manuf Processes 20:569
8. Datta S, Zhang Q, Sultana N, Mahfouf M (2013) Mater Manuf Processes 28(7):741
9. Mueller T, Kusne AG, Ramprasad R (2015) Rev Comput Chem (accepted for publication)
10. Rajan K (2013) Informatics for materials science and engineering: data-driven discovery for accelerated experimentation and application. Butterworth-Heinemann, Waltham

11. Horstemeyer MF (2012) Integrated computational materials engineering (icme) for metals: using multiscale modeling to invigorate engineering design with science. TMS—The Minerals, Metals and Materials Society. Willey, Hoboken

12. Thermocalc, http://www.thermocalc.com/solutions/by-application/alloy-development/ , accessed on **3/1/2015**

13. Jha R, Sen PK, Chakraborti N (2014) Steel Res Int 85:219

14. Jha R, Dulikravich GS, Pettersson F, Saxen H, Chakraborti N (2014) In: ASME symposium on elevated temperature application of materials for fossil, nuclear, and petrochemical industries, Seattle, WA, 25–27 March 2014, ETS2014-1008

15. Jha R, Dulikravich GS, Fan M, Shwartz J, Koch C, Egorov I, Poloni C (2014) In: CONEM 2014, Uberlandia, Brazil, 10–15 August 2014

16. Jha R, Pettersson F, Dulikravich GS, Saxen H, Chakraborti N (2015) Mater Manuf Processes 30(4):488

17. Toda-Caraballo I, Rivera-Diaz-Del-Castillo P (2015) JOM 67:108

18. Settouti N, Aourag H (2015) JOM 67:87

19. Spencer PJ (2008) CALPHAD: Comput Coupling Phase Diagrams Thermochem 32:1

20. Balamurugan B, Das B, Zhang WY, Skomski R, Sellmyer DJ (2014) J Phys: Condens Matter 26(6):064204

21. Factsage, http://www.factsage.com/ . Accessed on 3 Jan 2015

22. ESTECO:modeFRONTIER, http://www.esteco.com/modefrontier . Accessed on 3 Jan 2015

23. Colaço MJ, Orlande HRB, Dulikravich GS (2006) J Braz Soc Mech Sci Eng 28(1):1

24. Dulikravich GS, Colaço MJ (2015) Advances in evolutionary and deterministic methods for design, optimization and control in engineering and sciences. Springer, Heidelberg

25. Sobol IM, Comput USSR (1967) Maths Math Phys 7:86

26. Pettersson F, Saxen H, Chakraborti N (2007) Appl Soft Comput 7(1):387

27. Giri BK, Pettersson F, Saxen H, Chakraborti N (2013) Mater Manuf Processes 28(7):776

28. IBMSPSS http://www-01.ibm.com/software/analytics/spss/ . Accessed on 3 Jan 2015

29. Rettig R, Ritter NC, Helmer HE, Neumeier S, Singer RF (2015) Modell Simul Mater Sci Eng 23(3):035004